A New Mechanism for Hydroxyl Radical Production in Irradiated Nanoparticle Solutions

DOI:
10.1002/smll.201400110

Document Version
Final published version

NANO MICRO small

Nanoparticle Solutions

A New Mechanism for Hydroxyl Radical Production in Irradiated Nanoparticle Solutions

*Cécile Sicard-Roselli, Emilie Brun, Manon Gilles, Gérard Baldacchino, Colin Kelsey, Harold McQuaid, Chris Polin, Nathan Wardlow, and Frederick Currell**

The absolute yield of hydroxyl radicals per unit of deposited X-ray energy is determined for the first time for irradiated aqueous solutions containing metal nanoparticles based on a "reference" protocol. Measurements are made as a function of dose rate and nanoparticle concentration. Possible mechanisms for hydroxyl radical production are considered in turn: energy deposition in the nanoparticles followed by its transport into the surrounding environment is unable to account for observed yield whereas energy deposition in the water followed by a catalytic-like reaction at the water-nanoparticle interface can account for the total yield and its dependence on dose rate and nanoparticle concentration. This finding is important because current models used to account for nanoparticle enhancement to radiobiological damage only consider the primary interaction with the nanoparticle, not with the surrounding media. Nothing about the new mechanism appears to be specific to gold, the main requirements being the formation of a structured water layer in the vicinity of the nanoparticle possibly through the interaction of its charge and the water dipoles. The massive hydroxyl radical production is relevant to a number of application fields, particularly nanomedicine since the hydroxyl radical is responsible for the majority of radiation-induced DNA damage.

C. Sicard-Roselli, E. Brun, M. Gilles
Laboratoire de Chimie Physique CNRS UMR8000
Université Paris-Sud
91405 Orsay Cedex, France
G. Baldacchino
CEA Saclay, IRAMIS, LIDyl
Physico-Chimie et Rayonnement
UMR3299, CEA-CNRS 91191, Gif-sur-Yvette Cedex, France
C. Kelsey, H. McQuaid, C. Polin, N. Wardlow, F. Currell
Centre for Plasma Physics
School of Mathematics and Physics
Queen's University Belfast
BT7 1NN, UK
E-mail: f.j.currell@qub.ac.uk

DOI: 10.1002/smll.201400110

1. Introduction

Understanding the interaction between ionizing radiation and nanoparticles containing heavy atoms is important because such nanoparticles are being widely considered as dose-enhancing agents in cancer radiotherapy. Furthermore it has also been suggested that it could be relevant to application areas including nuclear waste handling, radiation chemistry and catalysis.[1] Both in vitro and in vivo experiments[2–8] have shown radiation enhancement effects due to the presence of nanoparticles although a consistent picture of the mechanisms at work is yet to emerge. Initial models accounting for the dose enhancement in cells considered only the physical dose increase[9,10] and more recent ones[11–13] the localized effect of a cascade of Auger-electron emissions. However these results were unable to account for the large enhancements typically observed. The essential feature of all

of the models presented to date is that the primary interaction occurs between the incoming radiation and the nanoparticle. In solution hydroxyl radicals (HO•) were proposed to be the main species responsible for biological damage in the presence of metallic nanoparticles.[14] This suggestion motivated studies where HO• production was determined when aqueous samples containing gold nanoparticles (GNPs) were irradiated.[1,15] Indeed, HO• production is important because between 50% and about 70% of DNA damage produced in standard radiotherapy upon X-ray irradiation is mediated by HO• radicals, depending on the conditions.[16] However, without absolute quantification of the hydroxyl overproduction in terms of a G-value, it is impossible to make meaningful comments regarding potential benefits of observed effects in treating cancer. The G-value is the number of moles of the substance produced per Joule of X-ray energy deposited in the sample and accordingly it carries the units of mol J^{-1}. Furthermore determining G-values provides an absolute basis for comparison across different studies to design the most efficient radiosensitizing nanoparticles, that is, metal type, size, coating and the radiation type and energy. In this paper we introduce a generic protocol able to quantify the production of HO• in the presence of nanoparticles and using this protocol we give the first quantification of the G-value for hydroxyl radical production as a function of nanoparticle concentration. The measured G-value and its change as a function of nanoparticle concentration also facilitate the framing of quantified arguments about mechanisms in terms of energetics.

Mechanisms able to produce HO• when nanoparticles are irradiated in aqueous media are shown in **Figure 1**. Energy can first be deposited either in the nanoparticle or the water. If the energy is first deposited in the nanoparticle, this alone cannot produce HO•. The energy must become available to break H-OH bonds, that is, energy must be transferred into the water through the emission of some species (electrons, holes or lower energy photons, pathway A). If the energy is first deposited in the water, it can then produce HO• without interactions involving the nanoparticle (pathway B, traditional water radiolysis) or through some interaction with the nanoparticle (pathway C). Our measurements in conjunction with arguments about the energetics of the system have allowed us to propose that pathway C is dominant for HO• production, at least in the specific system considered.

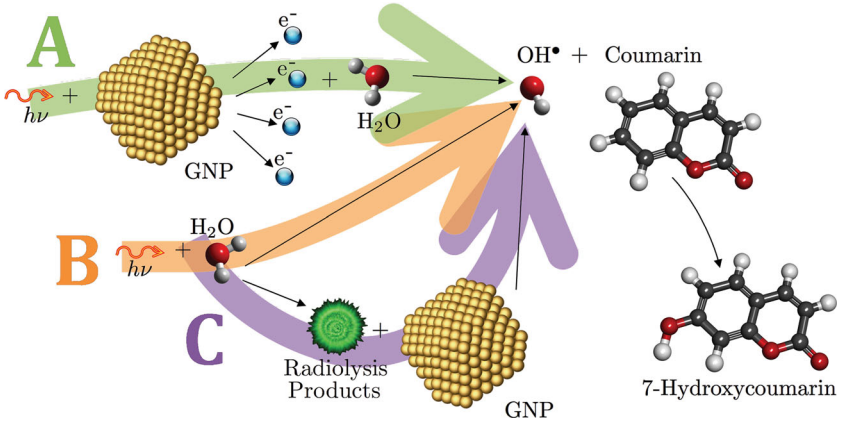

Figure 1. A schematic diagram of the pathways to form and determine the yield of the hydroxyl radical HO• in an irradiated solution containing gold nanoparticles. In pathway A, the primary interaction is with the nanoparticle, leading to photon, hole and electron emission. The energy transferred into the water then forms HO•. In pathway B, the photon interacts with the water to produce HO• but without interaction with the nanoparticle. In pathway C, the photon interacts with the water to produce a range of excited species some of which then diffuse to the water-nanoparticle interface where their excitation energy is used to produce HO•. In all cases, the HO• then goes on to interact with coumarin in the bulk water to form 7-hydroxycoumarin with a characteristic branching ratio. This final product is amenable to detection by fluorescence spectroscopy.

2. Results

Development of a new reliable protocol to quantify hydroxyl radicals was a key step to obtain $G_{HO•}$ values in the presence of gold nanoparticles. The quality of the assay used is demonstrated through the results shown in **Figures 2–5**, the important results leading to new insights about the mechanism being those presented in **Figures 6** and **7**.

2.1. Reliable Determination of the Yield of HO• in the Presence of Nanoparticles

2.1.1. Overview

The main methodological goal of this work was to establish a "reference" protocol for hydroxyl radical quantification in the presence of nanoparticles. We were particularly concerned by any source of discrepancy coming from the nanomaterial and irradiation apparatus: every batch of nanoparticles was fully characterized in terms of size, size distribution and charge before pooling, and the final suspensions were checked again (Figure 2). As recommended recently,[17] results from complementary techniques such as UV-visible measurements, dynamic light scattering (DLS) and transmission electron microscopy (TEM) were compared to give a more comprehensive view of their physicochemical properties. The nanoparticles were also extensively washed to remove as much of remaining citrate as possible and its oxidation products as they could induce an underestimation of HO• as alcohols are well-known hydroxyl radical scavengers. The irradiation conditions were designed to minimize possible systematic errors leading to a misestimation of hydroxyl radical production; our 'hanging drip' method (see below) minimizes the absorption by the apparatus and the contact area between the sample and any apparatus or container.

2.1.2. Coumarin Assay Adapted to Nanoparticle Solutions

32.5 nm nanoparticles were put in the presence of coumarin to measure the hydroxyl radical production after irradiation as it was suggested to be the main

small 2014,
DOI: 10.1002/smll.201400110

NANO MICRO small

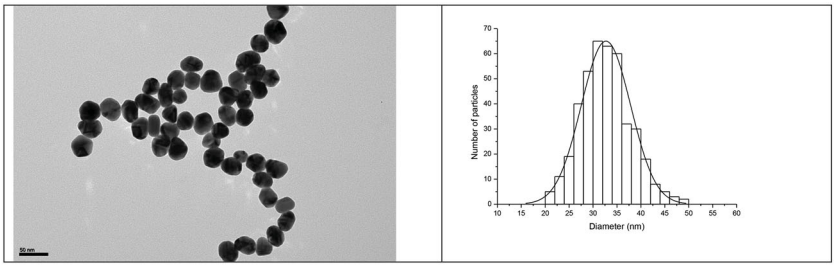

Figure 2. TEM characterization of GNP (left) and size distribution (right) of the 32.5 nm citrate stabilized nanoparticles used in this study. In the panel on the right the scale bar indicates 50 nm.

radical responsible for target degradation when nanoparticles are irradiated by ionizing radiation.[14] Among the numerous ways of quantifying hydroxyl radical production, the coumarin HO• trapping assay[18–20] was chosen because it is fully compatible with nanoparticles as it doesn't induce any aggregation and because fluorescence detection that can be run is a very sensitive technique allowing the detection of quantities down to 30 nM of hydroxyl radical.[21]

Louit et al performed HO• quantification by titration of 7-hydroxycoumarin that was shown to be the main fluorescent product of coumarin oxidation. This titration was validated both by liquid chromatography coupled to fluorescence detection and by fluorescence titration without preliminary separation of the oxidized coumarin derivatives. To validate our quantification in the presence of nanoparticles, our first concern was to exclude any interference caused by the presence of nanoparticles. Therefore we first compared the chromatographic profiles of irradiated solutions of coumarin in the presence or absence of gold nanoparticles. The HPLC profiles are very similar because the same oxidized coumarins are all present in both conditions (peaks from 12 to 26 min) but with different intensities (Figure 3). Peaks were attributed as labelled by comparison of standard oxidized coumarin injected under the same chromatographic conditions. Significant increases in the intensity of 7- and 5/8- hydroxycoumarins were observed when nanoparticles were present in solution. This evidences the fact that gold nanoparticles perturb HO• regioselectivity on coumarin. Nevertheless regioselectivity was observed to be independent in the range of concentrations studied. Then direct comparison of the signal intensity attributed to 7-OH coumarin obtained in water and for one colloidal concentration cannot be used to determine HO• yield of formation as the mechanism, and hence regioselectivity, is different in both cases. But by measuring the fluorescence of 7-OH coumarin as a function of nanoparticle concentration, it is possible to extract HO• production in the presence of nanoparticles.

There is a possible quenching of the 7-hydroxycoumarin signal by GNP as has already been observed for coumarin 152[22] and 153.[23] Therefore, irradiated samples of coumarin up to 150 Gy were incubated with 1 nM of GNPs for various times. In each case, after the incubation time has elapsed, contact was stopped by dilution in a 1% (w/v) NaCl solution to induce NP aggregation. When NaCl is added into a colloidal gold solution, nanoparticles aggregate and rapidly precipitate. The solution turns colourless and black spots can be clearly seen precipitating out, testifying of the disappearance of colloidal state. For our quenching experiments (see Figure 4), we checked that there was no more quenching in this aggregated state. The very large reduction of the surface area of gold could explain this phenomenon. The calibration curve for water samples without GNPs was submitted to the same treatment with no change in fluorescence intensity being

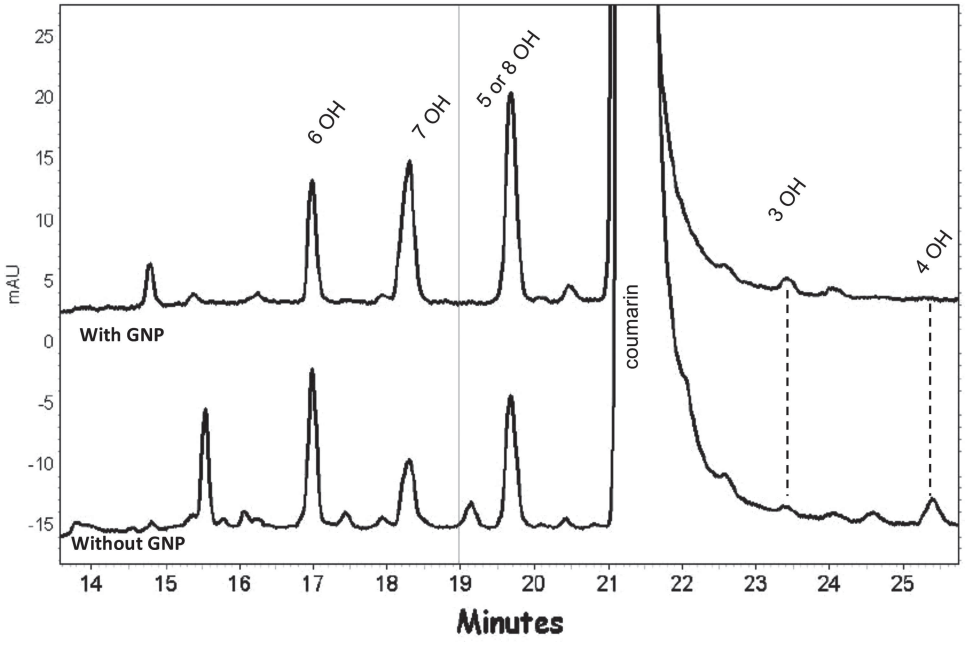

Figure 3. Chromatographic profiles of coumarin oxidized in the presence or absence of nanoparticles. Detection at 275 nm.

DOI: 10.1002/smll.201400110

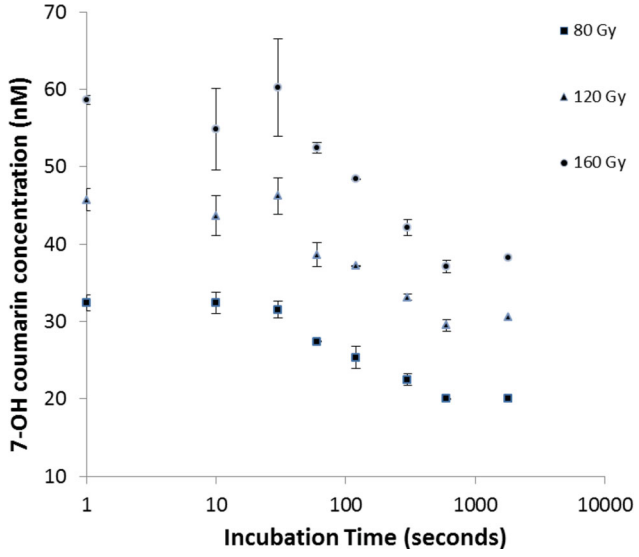

Figure 4. Influence of the nanoparticle time of contact with oxidized coumarin on the 7-OH coumarin fluorescence signal. Incubation up to 30 min with 1 nM nanoparticles of 32.5 nm diameter. Average and error bars of three independent experiments are presented.

observed in this case. Figure 4 shows the fluorescence signal detected at 456 nm after irradiation with doses of 80, 120, and 160 Gy, after different incubation times. This figure confirms that for short times (i.e., less than 30 s of incubation), 1 nM of gold nanoparticles do not induce any modification in the fluorescence intensity. Nevertheless, at times greater than 30 s a significant intensity decrease is observed, leading to a maximum of 30% decrease. To obtain quantitative measurements we ensured in all subsequent experiments that the irradiation time was less than 30 s after which contact of the sample with the GNPs was stopped by dripping the sample into a NaCl solution to induce NP aggregation.

The data illustrated in Figures 3 and 4 make it safe to assume that provided the change in regioselectivity due to the presence of GNPs is taken into account, fluorescence measurement of 7-hydroxycoumarin represents a quantitative measurement of $HO^{\bullet}$ radical production in the presence of GNPs when submitted to ionizing radiation.

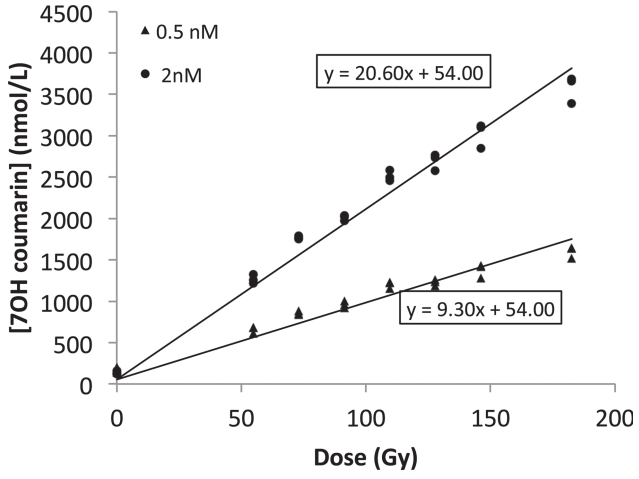

Figure 5. 7-OH coumarin formation as a function of the dose for 0.5 and 2 nM of nanoparticles for 20 keV at 12 Gy.s^{-1}.

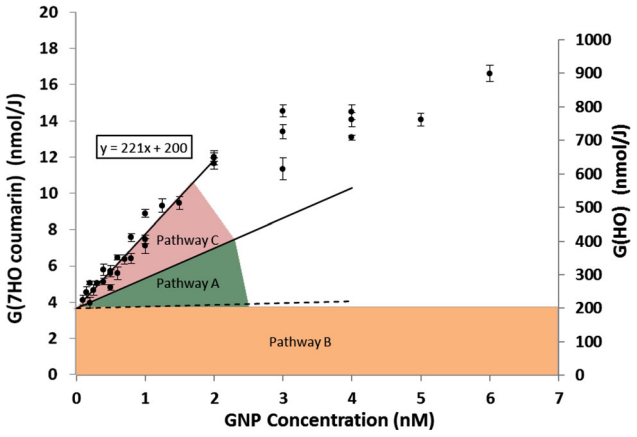

Figure 6. Measurements showing the yield of 7-hydroxycoumarin per Joule of radiation deposited in the sample (left *y*-axis) as a function of GNP concentration and a dose rate of 12 Gy s^{-1}. Through normalization to the known value of the yield/energy for the formation of hydroxyl radicals this has been converted to the yield/energy of hydroxyl radicals as a function of GNP concentration (right *y*-axis). The dashed line shows an upper bound for the predicted dependence at low concentration for pathway A of Figure 1, assuming emitted particles induce radiolysis in water in the usual way. The solid line shows the upper bound for the predicted dependence at low concentration assuming all the energy absorbed in the nanoparticle is transformed into hydroxyl. The intercept at [GNP] = 0 corresponds to the contribution from pathway B.

2.2. High Production of Hydroxyl Radical: Towards a New Mechanism

Figure 5 shows the fluorescence signal of 7-OH coumarin detected at 456 nm for two concentrations of NP (0.5 and 2.0 nM) as a function of the dose to water. This increase is linear and the slope represents the formation yield, or G-value, for 7-OH coumarin. The G-value is the number of moles of the substance produced per Joule of X-ray energy deposited in the sample. Over this range of dose and nanoparticle concentration, the increase in 7-OH coumarin production is linear with radiation dose, confirming that coumarin concentration does not represent a limiting factor.

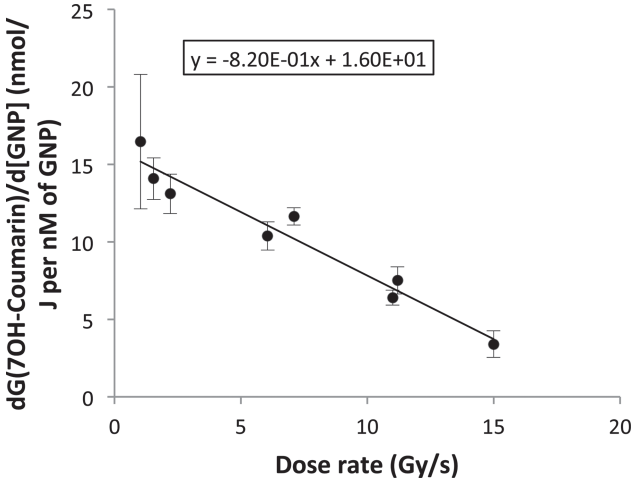

Figure 7. Rate of change of 7OH-Coumarin production with respect to gold nanoparticle concentration measured at various dose rates.

small 2014,
DOI: 10.1002/smll.201400110

NANO MICRO small

The results concerning the quantification of HO• at various nanoparticle concentrations are presented in Figure 6 in terms of G-values for the production of 7-OH coumarin (left-hand *y*-axis) and HO• (right-hand y-axis). The 7-OH coumarin production increases linearly with the molar concentration of nanoparticles up to 2 nM which is in agreement with previous results obtained on DNA.[2] At higher GNP concentration, we observe a slowing down of the slope. To convert $G_{7OH\ coumarin}$ into $G_{HO•}$, we extrapolated the formation yield of 7-hydroxycoumarin shown in Figure 6 to a concentration of 0 nM of GNPs (i.e., water alone) giving a value of $G_{7OHcoumarin} = 6.01 \pm 0.27$ nmol J^{-1}. As $G_{HO•} = 200$ nmol J^{-1} in water, the reaction yield of HO• with 0.5 mM coumarin to produce 7-OH coumarin in the presence of gold nanoparticles for 20 keV X-ray radiation with a dose rate of 12 Gy s^{-1} is ≈ 3.1%. This capture yield is in the same order of magnitude of a few percent as the one determined by Louit et al.[19] From the literature, we know that HO• radicals yield of formation for a X-ray beam at 20 keV after 1 μs is $G_{HO•} = 200 \pm 25$ nmol J^{-1}.[24] Yet the capture reaction of HO• radical by coumarin is known to be limited by diffusion with a rate constant of $k = 1.05 \times 10^{10}$ M^{-1} s^{-1}.[19]

$$COU + HO^{\cdot} \xrightarrow{k=1,0.5.10^{10}\ M^{-1}\ s^{-1}} COU-OH^{\cdot} \quad (1)$$

We can then write the expression giving $G_{HO•}$ at 20 keV photons for a dose rate of 12 Gy s^{-1} and in the range 0–2 nM of GNP, as $G_{HO•} = 200 + (221 \pm 9) \times$ [GNP] nmol J^{-1} where [GNP] is given in nM.

As G-values can be influenced by the dose rate of the incident radiation, the impact of the dose rate of the monoenergetic X-ray beam on our results was tested in the range 0.9 to 15.6 Gy s^{-1} (Figure 7). As before, for each dose rate, we measured the 7-HO coumarin fluorescence signal for different doses, plotted the $G_{7OHcoumarin}$ as a function of the GNP concentrations in the concentration range 0–2 nM of GNP. The HO• production is observed to decrease linearly with dose rates over the range studied as is illustrated in Figure 7. For each of the dose rates measured at the synchrotron, samples of coumarin (i.e., with no nanoparticles) were also irradiated and analysed. No statistical difference was observed in the yield of 7-HO coumarin across the range 1.5 to 15 Gy s^{-1} implying that $G_{7OHcoumarin}$ is either constant or very slowly varying across this range of dose rates.

3. Discussion

Due to the adaptation of the coumarin HO• trapping assay, we quantified for the first time hydroxyl radicals production in the presence of gold nanoparticles in terms of a G-value. This production is particularly high and suggests a very efficient process. The quantitative nature of our protocol allows us to compare our results to proposed mechanisms in the literature and eventually to make statements about the mechanisms at work.

Recently, Cheng et al.[1] proposed that the nanoparticles in excited states interact directly with some derivative of coumarin, each of these species having been created by interaction with an X-ray. This mechanism relies on two interactions with photons, one to create GNP* and one to create the derivative of coumarin (we will call cou'). However, this type of mechanism is hard to reconcile with our observed dose rate dependence. If GNP* and cou' are created by separate photons then one can consider the whole process as second order in photon rate which would lead to an increase of HO• production as the dose rate increases. This is contrary to our observations. Whilst Cheng et al. see an increase of HO• production enhancement with dose rate in the high dose plateau,[1] it is not clear from their data as presented if the initial slope (i.e., at low concentrations) has a dose rate dependence. Alternatively, GNP* and cou' could be created by the same initiator photon or its daughter products. In this case the rate of HO• production would be expected to be independent of dose rate, again contrary to our observation. Hence we can conclude this mechanism is not consistent with our observed dose rate dependence. This leads us to consider the three different pathways of Figure 1.

3.1. Consideration of Pathway B

Referring to Figure 1, Pathway B does not involve any interaction with the gold nanoparticles and therefore produces a constant yield of 200 nmol.J^{-1} of HO• regardless of gold concentration.[24] It leads to a constant hydroxyl radical production, as shown by the horizontal line in orange in Figure 6.

3.2. Consideration of Pathway A

Pathway A involves a primary interaction with the nanoparticle followed by energetic transfer into the media. For 32.5 nm diameter nanoparticles, there are about 1 million gold atoms per nanoparticle, assuming a particle density of 59 atoms nm^{-3}.[25] Taking the mass energy absorption coefficients for gold and water at 20 keV to be 6.522×10^1 cm^2 g^{-1} and 5.503×10^1 cm^2 g^{-1} respectively,[26] the fractional extra X-ray energy absorption for a sample containing 1 nM of these nanoparticles (equivalent to a mass fraction of 2.07×10^{-4}) is then given by $2.07 \times 10^{-4} \times 6.522 \times 10^1/5.503 \times 10^{-1} = 0.025$, that is, a fractional increase in X-ray energy deposited in the sample of 0.025 per nM of GNPs. Some proportion of this energy will then leave the nanoparticle in the form of photo- and Auger electrons, holes and lower energy photons. Some of the energy will be retained inside the nanoparticle as the electrons loose energy by scattering from other atoms in the nanoparticle on their way from the absorption site so the energy transferred into bulk water is less than this.

We can first consider that the extra energy absorption by the gold produces more HO• through known water radiolysis. In this case, the increase in HO• production is simply proportional to the increased energy absorption. Considering a scenario where all this extra energy is then transferred into water and is used for radiolysis ($G_{HO•}$ is equal to 200 nmol J^{-1}[24], we can estimate the HO• concentration generated as a function of the nanoparticle concentration. This then gives

DOI: 10.1002/smll.201400110

rise to an upper bound slope of 0.025 × 200 = 5.0 nmol J^{-1} per nM of GNP. This corresponds to the dashed line shown in Figure 6. Clearly this value is too low to account for the production of HO• observed.

Since the extra physical absorption by the gold coupling into standard radiolytic pathways in water is insufficient to account for the enhancement to the HO• yield observed, some more efficient mechanisms must be considered, that is, the photons, electrons and holes leaving the nanoparticle produce HO• in some other fashion than is known to occur in bulk water. Taking the molecular bond dissociation energy of 118.82 kcal mol^{-1} for the H-OH bond[27] and assuming a maximum possible value for the quantum yield of 1.0 gives an upper bound for the increase in $G_{HO•}$ due to simple H-OH bond breaking of 2022 nmol J^{-1} per nM of GNP (energy absorbed in the nanoparticle) for the reaction H_2O + Energy → HO• + H•. This value is still too low to account for our experimental data. More efficiently, the reaction might proceed as H_2O + Energy → HO• + ½ H_2, either in one step or a set of sequential steps. Taking the bond dissociation energies of 118.82 kcal mol^{-1} for the H-OH bond and 104.2 kcal mol^{-1} for the H-H bond[27] gives an energy cost for HO• production of 66.7 kcal mol^{-1} or 3583 nmol J^{-1} per nM of GNP (energy absorbed in the nanoparticle) for the upper bound on the increase in $G_{HO•}$ for the production of HO•. When considering the total energy absorbed in the sample (i.e., the ordinate of Figure 6), this corresponds to 90 nmol J^{-1} per nM of GNP. This corresponds to the solid line shown in Figure 6. This value is still too low to account for our observations by greater than a factor of two. Therefore absorption by the nanoparticle followed by a highly efficient bond breaking cannot account for the observations.

3.3. Consideration of Pathway C: Role of the Water-Nanoparticle Interface

As the extra absorption by the gold is small, most of the energy of the primary radiation is deposited into bulk water. We note that interactions with the nanoparticle must be invoked of necessity to produce a contribution other than that already accounted for by pathway B.

From the slope of Figure 6, 1 nM of GNP produces 221 nmol of additional HO• for a dose of 1 Gy compared to water. Taking into account the additional fraction of energy absorbed (0.025) we can calculate $dG_{HO•}/d[GNP]$ to be 221/0.025 = 8840 nmol J^{-1} per nM of GNP where only the extra energy absorbed by the nanoparticle is considered. Such an efficiency suggests a totally different mechanism, that is, pathway C of Figure 1. In this mechanism, the water-nanoparticle interface is thought to play a major role.

It is interesting to speculate about the details of the catalytic mechanism at the water-nanoparticle interface. Structured water layers are known to occur at water-solid interfaces[28] and also at water-nanoparticle interfaces.[29] Since the water layer is structured, it follows that there are additional hydrogen bonds pulling along the H-OH bonds in the dissociative direction acting to lengthen and weaken the intramolecular bonds. Since these bonds could be already strained, the injection of energy is likely to break them, leading to efficient production of HO•. The requirement for the formation of a structured water layer at the nanoparticle surface is simply that the nanoparticle has sufficient charge to align the water dipoles in its vicinity. This alignment and the hydrogen-bonds occurring between the water molecules will act together to produce the required structuring of water along with weakening of the H-OH bonds. This will then lead to the favourable formation of HO• observed. In other words, water radiolysis could be much more efficient in the vicinity of nanoparticles.

As nanoparticles are known to be responsible for several reactions, we can also propose the involvement of energy-carrying species produced through a primary interaction with water and diffusing to the water-nanoparticle interface where HO• is produced. For example, H_2O_2 was shown to dissociate into HO• at metallic nanoparticles surface.[30–32] A similar mechanism was studied in details by Jonsson and coll on metal oxide surfaces: they emphasized the importance of the HO• radical as an intermediate species in the decomposition of H_2O_2 and showed that the energy barrier for O–O cleavage is significantly lowered at the ZrO_2 surface (33 instead of 208 kJ mol^{-1}).[33] They also demonstrated that scavenging of HO• can occur at the particle surface, which confirms us the importance of eliminate of much citrate molecules as possible.[34] It then appears that a radiolytic molecular species could produce hydroxyl radical through nanoparticle catalysis.

In all cases, our experimental findings are in line with pathway C. In this model there is a competition between energy dissipation by other processes and the time to "find" a nanoparticle. At low nanoparticle concentrations, the time to find a nanoparticle decreases linearly with the concentration, giving rise to the observed linear trend in $G_{HO•}$. At higher concentrations the catalysis-involved species will rapidly find a nanoparticle before appreciable dissipation of the energy can occur. Based on this consideration, in the limit of very high concentration the value of $G_{HO•}$ is expected to tend to some asymptotic limit. This is in line with our observation at higher concentrations as is shown in Figure 6 where there is a clear departure from the linear onset towards a lower slope. Moreover, since the creation of HO• in this pathway is expected to happen at or near to the nanoparticle surface, there could be regions of high HO• density (i.e., just off the surfaces) and this density is supposed to increase with increased dose rate. Recombination could then take place with a high probability, in a manner rather analogous to the recombination found in heavy ion tracks,[35] reducing the amount of HO• entering the bulk water. This then leads to the prediction that the production rate of HO• decreases with dose rate, in line with our observations shown in Figure 7.

3.4. Biological Relevance

Due to the central role of the HO• radical in producing DNA damage, the relevance of our in vitro study of HO• produced by gold nanoparticles should be considered in a biological context, especially if one thinks to radiosensitization.

DOI: 10.1002/smll.201400110

NANO MICRO small

A GNP concentration of 1 nM induces the formation of an extra 221 nmol J^{-1} of hydroxyl radicals. This concentration of GNPs should be compared to what is tolerated in vivo. A review of in vitro toxicity studies does not reveal any noticeable effect of GNP for sizes higher than 5 nm. Some contradictory results exist but the large majority of published works conclude to a very low cytotoxicity of GNP: for example, Pan et al. estimated the IC50 for 15 nm GNP after a 48 h exposure higher than 6300 μM in four different cell lines.[36] For comparison, 1.5 nM of the GNP we used equals 1600 μM of gold or 320 μg mL^{-1} or 9.10^{11} nanoparticles mL^{-1}. In their recent review, Khlebtsov and Dykman proposed that, excepted for nanoparticles of 1–5 nm in diameter, 10^{12} particles mL^{-1} is a concentration below which no toxic effect appears.[37] This suggests that 1 nM GNP which is compatible with biological conditions induces a significant production of $HO^{\bullet}$ radicals under irradiation. Second, considering a radiation dose of 10 Gy, generally used for radiotherapy treatments, combined with 1 nM GNP, should lead to the formation of ≈ 2 μM of $HO^{\bullet}$ radicals. This amount must be sufficient to induce irreversible damages in cells through induction of multiple strand breaks. Third, it is worth noting that the medical sources such as orthovoltage therapy units have a typical dose rate of 2 Gy min^{-1}, which would be an advantage in their combination with GNP injection if the observed dose rate dependence carries over to in vivo settings. We can then consider that the $HO^{\bullet}$ production in the presence of nanoparticles quantified in vitro confirms the major role that could be played by nano-objects for future radiotherapy.

Indeed the elucidation of the mechanisms able to produce $HO^{\bullet}$ upon irradiation of nanoparticles in an aqueous environment has a potential impact on the wider field of nanomedicine. X-ray imaging (either CT or conventional) is the most common form of diagnostic imaging and it is likely to remain a cornerstone of medical practice. As nanoagents are introduced into the body as part of medical practice they will inevitably also be subjected to ionizing radiation. If they facilitate high levels of $HO^{\bullet}$ production, as we have observed here, then this leads to an increased probability of mutagenesis through DNA damage. Hence, under these conditions the biological dose of an X-ray procedure might be elevated.

4. Conclusion

A new protocol for the quantification of $HO^{\bullet}$ production in irradiated solutions of nanoparticles has been used to give precise quantification of a large increased $HO^{\bullet}$ yield over a range of dose rates and for various nanoparticles concentrations. This protocol is transposable to any kind of nanoparticles and can help screening any nanoagent's ability to produce hydroxyl radicals, which could give valuable information during the development of new nanomaterials. To account for the massive $HO^{\bullet}$ production we observed, different possible mechanisms were examined. According to energetic considerations, we have postulated that the existence of structured water layers surrounding the nanoparticles leads to new pathway to create $HO^{\bullet}$ very efficiently. The proposed mechanism is consistent with the absolute yield of $HO^{\bullet}$, the dependence on nanoparticle concentration and the dose rate dependence observed. This underlines the importance of the water-nanoparticle interface when nanoparticle solutions are subject to ionizing radiation.

5. Experimental Section

Gold Nanoparticle Synthesis and Characterization: Gold nanoparticles were synthetized according to the Turkevitch method,[38] that is, reduction of 100 mL of a 10^{-3} M $KAuCl_4$ solution by 4.6 mL of 1% (w/v) tri-sodium citrate. Nanoparticles were then washed as in[2] by three cycles of centrifugation to remove most of citrate and chemical reactants. The morphology and size of NPs were determined by transmission electron microscopy (TEM). 3 μL droplet of the NP solution was cast on formvar/carbon-coated copper grids for 1 min, the excess of solution absorbed and the grid dried on air. Samples were imaged on a JEOL JEM-1400 microscope operating at 120 kV. Images were acquired using a postcolumn high-resolution (11 megapixels) high-speed camera (SC1000 Orius, Gatan) and processed with Digital Micrograph (Gatan) and ImageJ software.[39] Analysis of more than 430 particles allowed us to determine the diameter of the particles at 32.5 ± 5.7 nm (Figure 2) which is in good agreement with the position of the plasmon resonance at 530 nm and correlated size.[40,41] Dynamic light scattering and zeta potential measurements were performed on a Malvern NanoZS equipped with a 633 nm laser. For determination of the hydrodynamic diameter, a fixed concentration of 0.8 nM of nanoparticles and a fixed position of the detection lens were used to ensure reproducibility of measurements. For zeta potential measurements, a fixed voltage of 150 mV in dip cells was applied. After washing by several centrifugation steps, gold nanoparticles exhibit a hydrodynamic diameter of 44 ± 3 nm and their zeta potential was found to be about −35 mV. These values are similar to those reported in the literature[42,43] with the small differences possibly being explained by some residual chemicals at the surface such as citrate for example. Taking into account its absorption coefficient ($\varepsilon = 3.98 \times 10^9$ L mol^{-1} cm^{-1}),[2] the nanoparticle concentrations can be calculated precisely. All concentrations in the text are thus expressed as moles of nanoparticles per liter. Assuming 59 atoms per nm^3, 1 nM of 32.5 nm GNP corresponds to 1.05 mM gold concentration or 2.1 10^{-2} wt%.

Coumarin and 7-Hydroxycoumarin Quantifications: Coumarin solution was prepared in water and irradiated at 0.5 mM in the presence of nanoparticles in a concentration range from 0 to 4 nM. As in,[19] coumarin oxidation products were separated from non-oxidized coumarin using HPLC (Beckman 168) in reverse phase (Kromasil C18 5 μm 250 × 4.6 mm) with a gradient between two elution buffers A (89% water, 10% methanol and 1% acetic acid) and B (89% methanol, 10% water and 1% acetic acid). The samples were submitted to the following gradient with a 0.8 mL min^{-1} flow rate: 0% B during 5 min, 0–30% B in 5 min, 30–50% B in 20 min, 50-100% B in 5 min. The absorbance was simultaneously recorded at 265 and 325 nm. To identify some of the oxidation products of coumarin, 3-, 4-, 6- and 7-hydroxycoumarins were injected alone with the same gradient and flow rate. Their retention time and absorption spectra were recorded to facilitate their identification in the separation profile of irradiated coumarin solution. Quantification of 7-hydroxycoumarin fluorescence was

DOI: 10.1002/smll.201400110

performed on a SpectraMax microplate reader (Molecular Device) at 25 °C. Excitation was set at 326 nm and emission spectra were recorded from 380 to 700 nm, with a maximum detected at 456 nm. Before any analysis, nanoparticles were removed from samples by centrifugation or by addition of salt to induce aggregation immediately after irradiation.

Irradiation: Irradiations of the samples were performed at the Diamond Light Source for irradiation at an energy of 20 keV. The dose rate was varied from 1 to 15.6 Gy s^{-1}. Two beamlines (B16 and I15) were used on separate occasions to provide the radiation with beam sizes of 5 mm by 5 mm typically being used. Samples were successively irradiated by expressing a small drip from a nozzle pointing vertically downwards. The drips were formed using a syringe pump controlled by a stepper motor. Previously the number of stepper motor steps required for a drip to fully form and then to fall downwards was carefully calibrated. Furthermore the mass of the drips was measured and found to consistently be 26.5 µg within 3%. Prior to irradiation a shutter upstream of the drip was closed. The drip was then expressed to the point just before it would fall from the nozzle after which the shutter was opened for a period of time chosen to deliver the required dose after which it was shut again. Then the syringe pump further expressed the drip so it fell into one well of a 96 well-plate, this event being detected with an opto-interupter (Omron EE-SX4070) that the drip past though. The 96 well-plate was mounted on a computer controlled x-y stage so that drips could be deposited into successive wells as required. This procedure was used for drips of sample, the corresponding controls and drips of the Fricke solution (see below). Throughout the irradiation process the alignment of the drip to the beam was checked using an X-ray eye. For the main experiments presented here GNP colloids at different concentrations were irradiated in the presence of 0.5 mM coumarin with 20 keV monochromatic X-rays. Each condition was repeated at least 4 independent times during each synchrotron beamtime and results obtained on the two different beamlines were consistent. Many sets of measurements like those shown in Figure 5 were made with each data set (corresponding to a different concentration of nanoparticles and/or dose rate) being fitted to the equation of a straight line using standard least-squares fitting techniques. The G-value for $HO^{\bullet}$ production, $G_{HO^{\bullet}}$, was deduced from the slopes to the fits. The errors used to produce Figure 6 and 7 were deduced from the reported uncertainties from the fitting process. For fluorescence quenching experiments, coumarin was irradiated with an X-ray generator (Enraf Nonius, Mo cathode) with increasing doses up to 150 Gy. Irradiated samples were incubated with GNP in a concentration range from 0 to 10 nM during times from 0 s to 1800 s, contact being stopped by dilution in a 1% (w/v) NaCl solution to induce NP aggregation. Samples were then analysed in fluorescence with the microplate reader. Three independent experiments were carried on to obtain the average and error bars presented.

Dosimetry: The extra absorption of the gold in each drip clearly increases as the concentration increases. A thin sample (compared to the attenuation length of the radiation) such as our drips, irradiated with 20 keV monoenergetic radiation and containing 1 nM of 32.5 nm diameter GNPs will absorb an extra 2.5% of radiation compared to the same drip containing water alone. This calculation indicates that the extra absorption due to the gold is small. There was a very small but measurable change in the absorption measured using a calibrated photodiode (PIPS PD300-500CB) directly traceable to the Physikalish-Technische Bundesanstalt standards. In principle one could calculate a correction to the dose scale to account for this effect to produce a scale showing dose to sample. However, this process would introduce both extra measurement and model uncertainties. Hence instead we report all results in terms of dose to water (i.e., the dose which would have been received by a sample of pure water in the same geometry under otherwise identical irradiation conditions) as measured by Fricke dosimetry. Hence, the dose scale was established chemically by using Fricke solution (0.4 M sulphuric acid, 6 mM ammonium ferrous sulphate and 1 mM potassium chloride) prepared with ultrapure water and well-agitated to guarantee oxygen saturation.[44] The oxidation of Fe(II) to Fe(III) was followed spectrophotometrically at 304 nm, considering a G-value of 1.43 µmol J^{-1} for Fe^{3+} at 20 keV.[44]

Acknowledgements

The authors acknowledge Diamond Light Source for time on beamlines B16, I15 and the side laboratories no. 67 under proposals MT9104, EE8481 and MT8482. The authors thank the beamline teams from both beamlines and other support staff who made these measurements possible. Samples were also analysed using equipment in the Research Complex at Harwell. Again, the authors thank the support staff who made this work possible. This work has benefited from the facilities and expertise of the Platform for Transmission Electronic Microscopy of IMAGIF (Centre de Recherche de Gif – www.imagif.cnrs.fr). The authors thank the French Embassy in the United Kingdom for providing travels funds to The Diamond Light Source to enable this collaboration to take place.

[1] N. N. Cheng, Z. Starkewolf, R. A. Davidson, A. Sharmah, C. Lee, J. Lien, T. Guo, *J. Am. Chem. Soc.* **2012**, *134*, 1950.
[2] E. Brun, L. Sanche, C. Sicard-Roselli, *Colloids Surf. B. Biointerfaces* **2009**, *72*, 128.
[3] K. T. Butterworth, S. J. McMahon, F. J. Currell, K. M. Prise, *Nanoscale* **2012**, *4*, 4830.
[4] K. T. Butterworth, J. A. Wyer, M. Brennan-Fournet, C. J. Latimer, M. B. Shah, F. J. Currell, D. G. Hirst, *Radiat. Res.* **2008**, *170*, 381.
[5] M. Y. Chang, A. L. Shiau, Y. H. Chen, C. J. Chang, H. H. Chen, C. L. Wu, *Cancer Sci.* **2008**, *99*, 1479.
[6] J. A. Coulter, W. B. Hyland, J. Nicol, F. J. Currell, *Clin. Oncol.* **2013**, *25*, 593.
[7] J. F. Hainfeld, D. N. Slatkin, H. M. Smilowitz, *Phys. Med. Biol.* **2004**, *49*, N309.
[8] S. Jain, J. A. Coulter, A. R. Hounsell, K. T. Butterworth, S. J. McMahon, W. B. Hyland, M. F. Muir, G. R. Dickson, K. M. Prise, F. J. Currell, J. M. O'Sullivan, D. G. Hirst, *Int. J. Radiat. Oncol. Biol. Phys.* **2011**, *79*, 531.
[9] S. H. Cho, *Phys. Med. Biol.* **2005**, *50*, N163.
[10] S. J. McMahon, M. H. Mendenhall, S. Jain, F. Currell, *Phys. Med. Biol.* **2008**, *53*, 5635.
[11] E. Lechtman, S. Mashouf, N. Chattopadhyay, B. M. Keller, P. Lai, Z. Cai, R. M. Reilly, J. P. Pignol, *Phys. Med. Biol.* **2013**, *58*, 3075.
[12] S. J. McMahon, F. Currell, Gold Nanoparticles for Imaging and Radiotherapy, in *Nanomedicine: nanotechnology, biology, and medicine* (Ed: H. Summers), Elsevier, Amsterdam, Holland **2013**.

DOI: 10.1002/smll.201400110

[13] S. J. McMahon, W. B. Hyland, M. F. Muir, J. A. Coulter, S. Jain, K. T. Butterworth, G. Schettino, G. R. Dickson, A. R. Hounsell, J. M. O'Sullivan, K. M. Prise, D. G. Hirst, F. J. Currell, *Sci. Rep.* **2011**, *1*, 18.
[14] J. D. Carter, N. N. Cheng, Y. Qu, G. D. Suarez, T. Guo, *J. Phys. Chem. B* **2007**, *111*, 11622.
[15] M. Misawa, J. Takahashi, *Nanomed. Nanotechnol. Biol. Med.* **2011**, *7*, 604.
[16] C. Von Sontag, *Free-radical-induced DNA damage and its repair. A chemical perspective,* Springer, Berlin **2006**.
[17] H. Hinterwirth, S. K. Wiedmer, M. Moilanen, A. Lehner, G. Allmaier, T. Waitz, W. Lindner, M. Lammerhofer, *J. Sep. Sci.* **2013**, *36*, 2952.
[18] S. Foley, P. Rotureau, S. Pin, G. Baldacchino, J. P. Renault, J. C. Mialocq, *Angew. Chem.* **2004**, *44*, 110.
[19] G. Louit, S. Foley, J. Cabillic, H. Coffigny, F. Taran, A. Valleix, J. P. Renault, S. Pin, *Radiat. Phys. Chem.* **2005**, *72*, 119.
[20] T. S. Singh, B. S. M. Rao, H. Mohan, J. P. Mittal, *J. Photochem. Photobiol., A* **2002**, *153*, 163.
[21] G. Louit, M. Hanedanian, F. Taran, H. Coffigny, J. P. Renault, S. Pin, *The Analyst* **2009**, *134*, 250.
[22] M. Fukushima, H. Yanagi, S. Hayashi, N. Suganuma, Y. Taniguchi, *Thin Solid Films* **2003**, *438*, 39.
[23] D. Ghosh, N. Nandi, N. Chattopadhyay, *J. Phys. Chem. B* **2012**, *116*, 4693.
[24] J. Fulford, H. Nikjoo, D. T. Goodhead, P. O'Neill, *Int. J. Radiat. Biol.* **2001**, *77*, 1053.
[25] C. Kittel, *Introduction to solid-state physics,* Wiley, New York **1996**.
[26] http://www.nist.gov/pml/data/xraycoef/ (accessed 7 May 2014).
[27] S. J. Blanksby, G. B. Ellison, *Acc. Chem. Res.* **2003**, *36*, 255.
[28] J. Carrasco, A. Hodgson, A. Michaelides, *Nat. Mater.* **2012**, *11*, 667.
[29] J. Soussi, S. Voltz, Y. Chalopin, *Thermal Properties of Functionalized Gold Nanoparticles for Hyperthermia presented at GdR(Groupe de recherche) meeting Or-nano* Nantes, France **2013**.
[30] Y. F. Han, N. Phonthammachai, K. Ramesh, Z. Zhong, T. White, *Environ. Sci. Technol.* **2008**, *42*, 908.
[31] A. Quintanilla, S. Garcia-Rodriguez, C. M. Dominguez, S. Blasco, J. A. Casas, J. J. Rodriguez, *Appl. Catal. B-Environ.* **2012**, *111*, 81.
[32] W. W. He, Y. T. Zhou, W. G. Wamer, M. D. Boudreau, J. J. Yin, *Biomaterials* **2012**, *33*, 7547.
[33] C. M. Lousada, M. Jonsson, *J. Phys. Chem. C* **2010**, *114*, 11202.
[34] C. M. Lousada, J. A. LaVerne, M. Jonsson, *Phys. Chem. Chem. Phys.* **2013**, *15*, 12674.
[35] S. Yamashita, M. Taguchi, G. Baldacchino, Y. Katsumura, Radiation chemistry of liquid water with heavy ions: steady-states and pulse radiolysis studies, in *Charged Particles and Photon Interactions with Matter. Recent advances, Applications and Interfaces*, (Eds: Y. Hatano, Y. Katsumura, A. Mozumder) CRC Press, Taylor and Francis Group, Boca Raton, FL **2011**.
[36] Y. Pan, S. Neuss, A. Leifert, M. Fischler, F. Wen, U. Simon, G. Schmid, W. Brandau, W. Jahnen-Dechent, *Small* **2007**, *3*, 1941.
[37] N. Khlebtsov, L. Dykman, *Chem. Soc. Rev.* **2011**, *40*, 1647.
[38] J. Turkevitch, *Gold Bull.* **1985**, *18*, 86.
[39] C. A. Schneider, W. S. Rasband, K. W. Eliceiri, *Nat. Methods* **2012**, *9*, 671.
[40] S. Link, M. A. El-Sayed, *J. Phys. Chem. B* **1999**, *103*, 4212.
[41] P. N. Njoki, I. I. S. Lim, D. Mott, H. Y. Park, B. Khan, S. Mishra, R. Sujakumar, J. Luo, C. Zhong, *J. Phys. Chem. C* **2007**, *111*, 14664.
[42] T. L. Doane, C. H. Chuang, R. J. Hill, C. Burda, *Acc. Chem. Res.* **2012**, *45*, 317.
[43] G. Sonavane, K. Tomoda, K. Makino, *Colloids Surf. B. Biointerfaces* **2008**, *66*, 274.
[44] J. W. T. Spinks, R. J. Woods, *Introduction to radiation chemistry* third ed.; Wiley New-York, **1990**.

Received: January 14, 2014
Revised: March 12, 2014
Published online: